pathologists according to the WHO classification updated in 2007. The Ki-67 LI was also calculated. All patients were followed up at our out-patient clinic without any additional treatment for the tumor during the follow-up period. For the surgical cases, gadolinium (Gd)-enhanced magnetic resonance imaging (MRI) was performed every 3–6 months in the first 2 years after surgery, and then every year during the follow-up period. For the observation cases, Gd-enhanced MRI was performed more than once a year. The mean follow-up period was 80 ± 52 months (range 4–180 months). In surgical cases, the lesion was defined as a 'recurrence' when a lesion was found at the same location or a residual lesion was obviously enlarged in the radiological examinations. In non-surgical observation cases, the lesion was defined as a 'progression' when the tumor size was obviously enlarged in the radiological examinations.

We evaluated the risk factors for recurrence and progression by age, gender, location (skull base or not), extent of resection (GTR or not), Ki-67 LI, and LN ratio of MET uptake.

Statistical analysis

We evaluated the risk factors for recurrence and progression using paired *t* tests. When the data were not normally distributed, Wilcoxon's rank-sum test was used for continuous data. Fisher's exact tests were used for categorical data. Cox proportional hazards regression analysis was used for the surgical cases to assess the predictors of recurrence and progression with duration of the recurrence-free period as the time variable. A receiver operating characteristics (ROC) curve was assessed to confirm the best cutoff value of the LN ratio for recurrence and progression. All statistical analysis was performed using JMP 9 software (SAS Institute Inc.).

Results

Characteristics and pathology

During the follow-up period, six surgical patients had a recurrence, and two observation patients progressed. The characteristics of the 37 cases are shown in Table 1. Summaries of the recurrence group and the non-recurrence group are shown in Table 2. The mean age of the recurrence group was 57.9 ± 11.8 years, and that of the non-recurrence group was 53.6 ± 13.2 years. We found no significant difference in the numbers of males and females in each group.

The tumor location is shown in Table 1. We classified the tumor location into two groups: skull base and non-skull base. The recurrence rate was not significantly different between these two groups.

Two patients died during the clinical follow-up period. One (case 20) died of thyroid cancer 51 months after PET examination, and another (case 21) died due to tumor progression 4 months after PET examination. The tumors were classified by pathology as follows. Ten were meningothelial (30 %), nine were fibrous (27 %), eight were transitional (24 %), two were angiomatous (6 %), two were chordoid (6 %), one was secretory (3 %), and one was atypical (3 %). Thirty cases were WHO grade I meningiomas, and three cases were WHO grade II meningiomas. The recurrence rate was not significantly different between WHO grade I (17 %, 5/30 cases) and grade II (33 %, 1/3 cases). The mean LN ratio of WHO grade I meningiomas was 2.99 ± 1.07, and the mean LN ratio of WHO grade II meningiomas was 2.35 ± 0.36. The LN ratio was not significantly different between WHO grade I and grade II.

Extent of tumor resection and recurrence

Gross total resection was performed in 18 patients, and one patient (case 35) had a recurrence during clinical follow-up. In 15 patients, some tumor remained after the surgery. In this non-GTR group, recurrence of meningioma was observed in five patients. The recurrence rate was not significantly different between the non-GTR group and the GTR group ($p = 0.053$).

LN ratio of MET PET and Ki-67 LI for progression and recurrence

During the clinical follow-up, six cases of recurrence and two cases of progression were found. The average LN ratio of these eight cases was 3.67 ± 1.15 [95 % confidence interval (CI) 2.71–4.64] and that of the remaining 29 cases was 2.65 ± 0.86 (95 % CI 2.32–2.98). The average LN ratio of the cases with recurrence and progression was higher than that of the cases without recurrence or progression ($p < 0.01$, Fig. 2). The average Ki-67 LI of the recurrent six cases was 1.81 ± 1.21 (95 % CI 0.54–3.09), and that of the 27 cases without recurrence was 3.06 ± 3.84 (95 % CI 1.54–4.58). The Ki-67 LI was not significantly different between the recurrence group and the non-recurrence group ($p = 0.44$). No correlation was found between the LN ratio and the Ki-67 LI (Fig. 3). Risk factors evaluated with univariate analysis are summarized in Table 2. One illustrative case is shown in Fig. 4.

Table 1 Characteristics of 37 patients with meningioma

No.	Age (years)	Gender	Location	Pathological diagnosis	WHO grade	Ki-67	LN ratio	Surgery	Recurrence/ progression (months after pet exam)	Follow-up (months)
1	48	F	Parasagittal	Transitional	I	15.5	2.23	GTR	No	176
2	67	F	Parasagittal	Transitional	I	3	2.22	GTR	No	45
3	49	F	Sphenoid ridge	Chordoid	II	1.34	2.63	GTR	No	157
4	57	F	Petroclival	Secretory	I	14.4	3.00	GTR	No	40
5	49	M	Olfactory groove	Transitional	I	4.98	2.63	GTR	No	180
6	39	M	Pineal	Chordoid	II	3.03	1.95	GTR	No	26
7	61	F	Clival	Fibrous	I	4	5.10	STR	Yes (9)	141
8	43	M	Parasagittal	Fibrous	I	0.3	3.97	GTR	No	159
9	58	F	Parasagittal	Fibrous	I	1.45	3.10	GTR	No	34
10	46	F	Convexity	Fibrous	I	4.49	3.73	GTR	No	88
11	61	M	Clinoidal	Transitional	I	1.12	2.94	STR	No	152
12	79	M	Convexity	Meningothelial	I	1.26	5.38	STR	Yes (13)	56
13	57	F	Parasagittal	Angiomatous	I	2.29	3.61	STR	Yes (20)	147
14	37	F	Convexity	Meningothelial	I	2.27	3.37	GTR	No	145
15	54	F	Tentorial	Fibrous	I	0.59	3.32	STR	No	142
16	71	M	Parasagittal	Meningothelial	I	0.92	5.09	STR	No	65
17	66	F	C-P angle	Transitional	I	0.49	2.65	STR	No	138
18	22	F	Convexity	Meningothelial	I	1.3	1.98	GTR	No	130
19	60	M	Sphenoid ridge	Fibrous	I	1.33	2.90	STR	Yes (17)	71
20	74	M	Tuberculum sellae	Meningothelial	I	0.2	2.17	STR	No	51
21	39	M	Middle fossa	–	–		3.18	–	Yes (4)	4
22	75	F	C-P angle	Fibrous	I	3.5	2.35	GTR	No	54
23	52	F	Tuberculum sellae	Angiomatous	I	1	2.54	GTR	No	110
24	50	F	Sphenoid ridge	Meningothelial	I	1.26	1.65	STR	No	29
25	49	F	C-P angle	–	–	–	1.53	–	No	97
26	62	M	Convexity	Fibrous	I	3	2.86	STR	No	65
27	57	M	Convexity	Transitional	I	2.95	1.20	GTR	No	48
28	44	F	Foramen magnum	Meningothelial	I	5.6	2.64	GTR	No	48
29	48	F	Intraventricular	Fibrous	I	6.5	3.03	GTR	No	74
30	42	F	Sphenoid ridge	Transitional	I	2	2.73	STR	No	69
31	62	F	Convexity	Transitional	I	0.1	1.68	Biopsy	No	47
32	30	F	Intraventricular	–	–	–	2.49	–	No	24
33	69	F	Convexity	Meningothelial	I	0.3	1.27	GTR	No	43
34	49	M	Clivotentorial	–	–	–	2.39	–	Yes (43)	43
35	53	F	Intraventricular	Atypical	II	1.5	2.48	GTR	Yes (26)	26
36	65	M	Clival	Meningothelial	I	0.5	4.35	Partial	Yes (15)	25
37	72	M	Tentorial	Meningothelial	I	1	3.89	STR	No	23

C-P angle cerebello-pontine angle, *GTR* gross total resection, *STR* subtotal resection

In our study, the LN ratio was a significant risk factor for recurrence and progression with univariate analysis. We also evaluated risk factors using multivariate analysis. The results are summarized in Table 3. Multivariate analysis showed that the LN ratio, the extent of resection, and the WHO grade were significant risk factors for recurrence and progression. The hazard ratio of the LN ratio was 4.21. The LN ratio was the only factor examined preoperatively.

ROC curve analysis

A ROC curve was generated, and the area under the curve (AUC) was calculated to determine the best discriminating

Table 2 Evaluation of risk for recurrence and progression using univariate analysis

	Total cases		Recurrence/progression	Non-recurrence/progression	*p* value
Cases	37		8	29	
Age (years)	37		57.9 ± 11.8	53.6 ± 13.2	0.41
Gender	37	Female	3	20	
		Male	5	9	0.22
Skull base	37	Yes	5	11	
		No	3	18	0.25
LN ratio	37		3.67 ± 1.15	2.65 ± 0.86	<0.01
Extent of resection	33	GTR	1	17	
		Non-GTR	5	10	0.053
WHO grade	33	Grade I	5	25	
		Grade II	1	2	0.46
Ki-67 LI	33		1.81 ± 1.21	3.06 ± 3.84	0.44

The LN ratio was a significant risk factor for recurrence and progression

LN lesion to normal, *GTR* gross total resection, *LI* labeling index

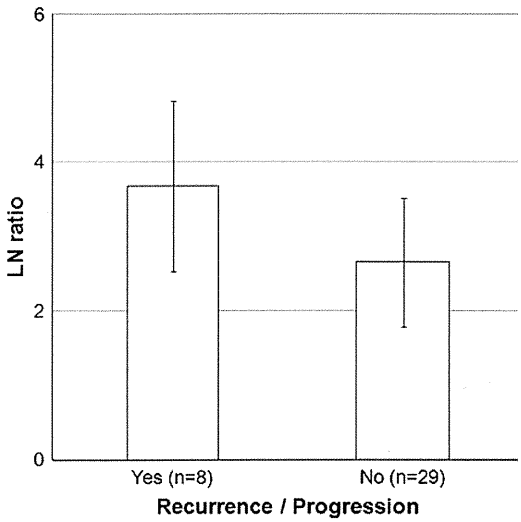

Fig. 2 LN ratio of MET PET and recurrence/progression. The LN ratio in cases with recurrence and progression was significantly higher than that in cases without recurrence and progression ($p < 0.01$)

level of the LN ratio for predicting recurrence and progression. ROC analysis confirmed 3.18 as the best predictive cutoff value of the LN ratio for recurrence and progression. The AUC was 0.754. Using the best cutoff value of 3.18, the sensitivity and specificity were 63 and 79 %, respectively (Fig. 5).

Discussion

The risk factors for recurrence and progression in meningioma have been reported in many previous studies. They include age [5, 6], gender [7], tumor size [8], calcification [7, 9], brain invasion [10], location [11], vascular density [12], Ki-67 LI [8, 13–15], extent of the resection [12, 16, 17], and WHO grade [11]. In our study, age, gender, tumor location, Ki-67 LI, and the LN ratio of MET PET were investigated. A high LN ratio was significantly correlated with tumor recurrence and progression. However, age, gender, tumor location, and KI-67 LI were not significantly correlated with tumor recurrence. These risk factors remain controversial.

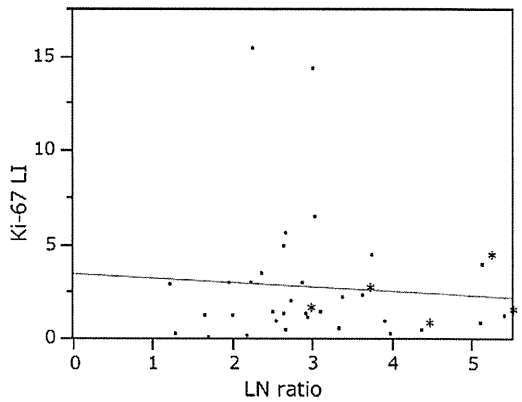

Fig. 3 Correlation between the LN ratio of MET PET and the Ki-67 LI. No correlation between the LN ratio and the Ki-67 LI was observed. *Asterisks* cases with recurrence or progression

Recently, the MET PET method has been used in gliomas and other intracranial tumors to evaluate the malignancy of the tumor and the proliferative activity. In previous studies of gliomas, MET uptake correlated with the WHO grade, Ki-67 LI, and patient survival [18–21]. However, the role of MET PET in meningioma is not clear. In a previous study using ^{18}F-fluorodeoxyglucose (FDG) PET, ^{18}F-FDG uptake was correlated with the Ki-67 LI but not with recurrence of the meningioma [22, 23]. Using

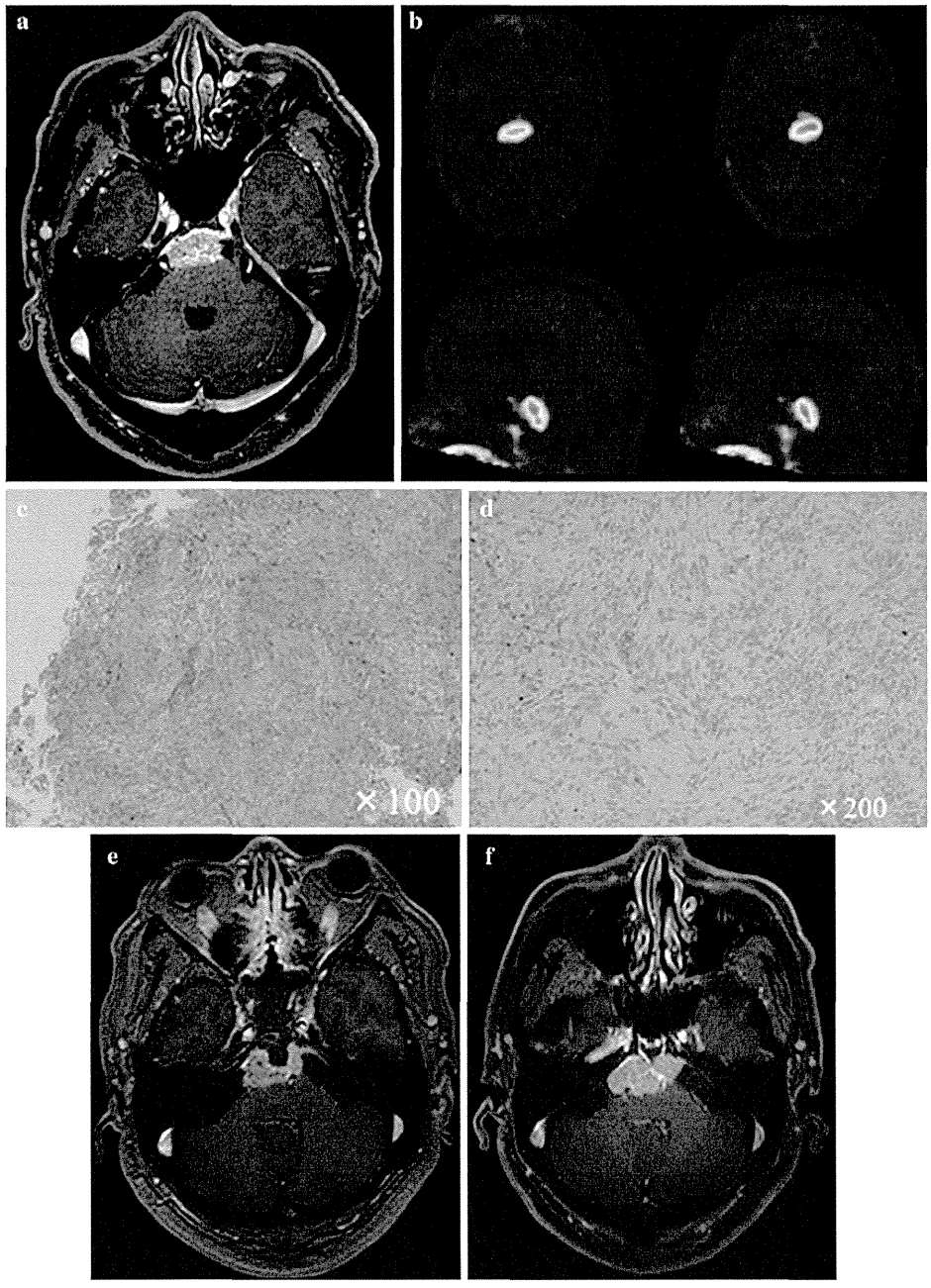

Fig. 4 Case 36. **a** Preoperative Gadolinium (Gd)-enhanced T1-weighted image. The tumor is located at the clivus. **b** ^{11}C-methionine was taken up into the tumor. The LN ratio was 4.35. **c**, **d** Photomicrograph of a sample of the lesion. Hematoxylin and eosin-stained section (**c** ×100) and Ki-67 staining (**d** ×200) of a meningioma tissue specimen. The diagnosis based on pathology was meningothelial meningioma. The Ki-67 LI was 0.5. **e** Postoperative Gd-enhanced T1-weighted image. In this case, the tumor was partially removed using a trans-sphenoidal approach. **f** Gd-enhanced T1-weighted image 15 months after surgery. The tumor had begun to grow again

kinetic analysis with ^{18}F-FDG PET, Tsuyuguchi [24] showed that the kinetic rate constant of glucose metabolism is related to the Ki-67 LI. However, that analysis requires frequent arterial blood samplings and dynamic PET scanning. The procedure is very complicated and not practical for clinical use. Moreover, the results of ^{18}F-FDG PET are influenced by blood glucose. In patients with hyperglycemia, the results may lead to overestimation [25]. Iuchi et al. [26] showed that MET uptake is significantly correlated with the count of nuclear organizer regions, which is a histological index of protein synthesis, the Ki-67 LI, and a histological index of proliferative activity. In that study,

^{18}F-FDG uptake showed no significant correlation with the Ki-67 LI or clinical malignancy. The uptake of methionine reflects amino acid transport and metabolism, but this does not mean that methionine uptake is correlated with protein synthesis and proliferation [27]. Some previous studies have shown that MET uptake correlates with microvessel density in glioma cases [28, 29], but in meningioma cases, MET uptake does not correlate with microvessel density [30]. This observation may reflect the fact that meningioma has multiple pathological subtypes and, thus, microvessel density may be different in each subtype. To evaluate the correlation between the LN ratio and microvessel density in meningioma, many cases of each subtype would be necessary.

Table 3 Evaluation of risk factors for recurrence using Cox proportional hazards model

	p value	Risk ratio
Age (years)	0.28	
Gender	0.43	
Skull base	0.12	
LN ratio	0.03	4.21
Extent of resection (non-GTR/GTR)	0.014	
WHO grade (grade II/grade I)	0.0074	
Ki-67 LI	0.079	

LN ratio, extent of resection, and WHO grade were significant risk factors

LN lesion to normal, *WHO* World Health Organization, *GTR* gross total resection, *LI* labeling index

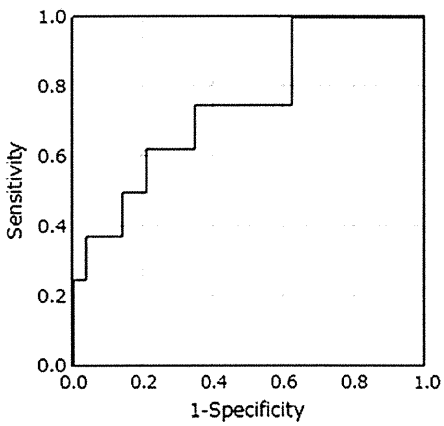

Fig. 5 ROC curve of the LN ratio. AUC of the LN ratio of MET PET was 0.754. The optimal cutoff value was 3.18. The sensitivity and specificity were 63 and 79 %, respectively

Arita et al. [30] showed that the LN ratio of MET uptake is not significantly correlated with tumor doubling time. In this study, many asymptomatic patients were enrolled, and the mean tumor doubling time was very long (174 ± 270 months) despite a short follow-up period (26.7 ± 16.7 months). Thus, evaluation of recurrence and progression in meningioma using tumor doubling time appeared to be difficult because most meningiomas progress slowly.

Compared with ^{18}F-FDG PET, the contrast between a meningioma lesion and normal brain tissue is clear in MET PET and, thus, we can correctly define the ROI using MET PET. Recently, we have evaluated MET uptake more correctly by fusing PET images with computed tomography or MR images.

In this study, we calculated the LN ratio using the mean MET uptake of the lesion and the normal brain tissue. The methionine uptake in the tumor depends not only on the metabolic rate, but also on the vascular bed [31]. The vascular bed of the meningioma is different within the various pathological types of meningiomas [32], and the vascular bed may be variable in the same specimen. Biological activity is heterogeneous in the same meningioma lesion [33, 34]. Thus, partially high MET uptake does not always indicate a high metabolic rate of the whole tumor. In this study, we used the mean MET uptake, not the maximum MET uptake, to reduce the influence on the heterogeneity of MET uptake.

Table 4 Evaluation of risk factors for recurrence and progression excluding gross total resection cases

Only the LN ratio was significantly different between the recurrence/progression group and the non-recurrence/progression group

LN lesion to normal, *WHO* World Health Organization, *LI* labeling index

	Total cases		Recurrence/progression	Non-recurrence/progression	*p* value
Cases	19		7	12	
Age (years)	19		58.6 ± 12.5	57.8 ± 13.2	0.9
Gender	19	Female	2	7	
		Male	5	5	0.35
Skull base	19	Yes	5	6	
		No	2	6	0.63
LN ratio	19		3.84 ± 1.13	2.74 ± 1.02	0.04
Surgical cases			5	10	
WHO grade	15	Grade I	5	10	
		Grade II	0	0	
Ki-67 LI	15		1.87 ± 1.35	1.06 ± 0.87	0.18

In this study, tumor progression and recurrence were not significantly different between the GTR and non-GTR groups. However, in some cases with a high Ki-67 LI, GTR was performed, and the recurrence rate was low. GTR was a factor that strongly influenced the recurrence rate. We evaluated the recurrence and progression in the non-GTR group. The LN ratio in the group with recurrence and progression was also significantly higher than that in the group without recurrence and progression ($p < 0.05$). The Ki-67 LI was not significantly different ($p = 0.18$). Our observations are summarized in Table 4.

In our study, the LN ratio was a significant risk factor for recurrence and progression. The LN ratio of MET PET may indicate the proliferative activity of meningioma. Using ROC analysis, the AUC was 0.754, and the best cutoff value was 3.18, resulting in a sensitivity and specificity of 63 and 79 %, respectively. The sensitivity and specificity of the LN ratio were not less than those of the Ki-67 LI, as described in a previous study [35, 36].

In our study, the Ki-67 LI was not significantly different between the patients with recurrence and those without. We also found no correlation between the LN ratio and the Ki-67 LI. Some previous papers have reported that the correlation between the Ki-67 LI and tumor recurrence is controversial [4, 33, 37, 38]. Meningioma is characterized by heterogeneous biological activity within the same tumor tissue [33, 34]. It is doubtful that the Ki-67 LI obtained from a small tumor specimen can adequately evaluate the proliferative potential of the whole tumor. In fact, MET uptake is heterogeneous in a large tumor and may reflect the heterogeneity of the Ki-67 LI. The MET PET method is useful for evaluating the whole tumor. The Ki-67 LI overlaps within each grade of meningioma [39–41]. Evaluating the proliferative activity of the whole tumor and providing an accurate prognosis may be difficult with only one index.

The extent of resection was a significant risk factor as shown in a previous study [12, 16, 17]. However, the location of the tumor was not a significant risk factor in this study. Sixteen cases of skull base meningioma were included. In these cases, total resection without complications is difficult. A GTR of the tumor would reduce the risk of recurrence. This result may indicate that additional treatments are necessary for a residual tumor in which the LN ratio is higher than 3.18.

The WHO grade of meningioma was also a significant risk factor. In this study, we investigated preoperative cases and, thus, most cases were WHO grade I; only three cases were WHO grade II. Cases with WHO grade III meningioma are relatively infrequent at initial diagnosis. Almost all cases of meningioma are pathologically benign. Thus, we have to follow patients for a long time to investigate malignant changes and the prognosis. We must investigate additional consecutive cases to evaluate the largest number and the widest variety of cases.

Our study showed that the MET PET method has useful sensitivity and specificity for evaluation of recurrence and progression in meningioma. The most beneficial point is that ^{11}C-methionine PET is not invasive, whereas analysis of the Ki-67 LI requires surgery. Thus, without surgery, we can evaluate the risk of progression and recurrence and consider the treatment strategy. We can determine the risk of progression and recurrence before deciding on observation or surgery. In asymptomatic cases, high LN ratio of MET PET may be the decisive factor for determining surgical treatment. We did not evaluate a large number of cases, and thus continued collection of cases and evaluation of the data are necessary.

Conclusion

The results of our study showed that MET uptake by the meningioma was a significant prognostic factor. MET uptake was significantly higher in cases with recurrence or progression. The AUC of the LN ratio for recurrence or progression was 0.754, and the best cutoff value was 3.18. The greatest advantage associated with the MET PET method is its non-invasive nature.

Acknowledgments The authors appreciate the technical support of the radiological technologist at our institute.

Conflict of interest The authors have no personal financial or institutional interest in any of the drugs, materials, or devices described in this article.

References

1. Committee of Brain Tumor Registry of Japan. Report of Brain Tumor Registry of Japan (1984-2000) Neurol Med Chir. 2009;49 Suppl.
2. Crompton MR, Gautier-Smith PC. The prediction of recurrence in meningiomas. J Neurol Neurosurg Psychiatry. 1970;33(1): 80–7.
3. Jellinger K, Slowik F. Histological subtypes and prognostic problems in meningiomas. J Neurol. 1975;208(4):279–98.
4. Roser F, Samii M, Ostertag H, Bellinzona M. The Ki-67 proliferation antigen in meningiomas. Experience in 600 cases. Acta Neurochir. 2004;146(1):37–44 (discussion).
5. McCarthy BJ, Davis FG, Freels S, Surawicz TS, Damek DM, Grutsch J, et al. Factors associated with survival in patients with meningioma. J Neurosurg. 1998;88(5):831–9.
6. Nakamura M, Roser F, Michel J, Jacobs C, Samii M. The natural history of incidental meningiomas. Neurosurgery. 2003;53(1):62–70 (discussion-1).
7. Niiro M, Yatsushiro K, Nakamura K, Kawahara Y, Kuratsu J. Natural history of elderly patients with asymptomatic meningiomas. J Neurol Neurosurg Psychiatry. 2000;68(1):25–8.

8. Kasuya H, Kubo O, Tanaka M, Amano K, Kato K, Hori T. Clinical and radiological features related to the growth potential of meningioma. Neurosurg Rev. 2006;29(4):293–6 discussion 296-297.
9. Kuratsu J, Kochi M, Ushio Y. Incidence and clinical features of asymptomatic meningiomas. J Neurosurg. 2000;92(5):766–70.
10. Alvernia JE, Dang ND, Sindou MP. Convexity meningiomas: study of recurrence factors with special emphasis on the cleavage plane in a series of 100 consecutive patients. J Neurosurg. 2011;115(3):491–8.
11. McGovern SL, Aldape KD, Munsell MF, Mahajan A, DeMonte F, Woo SY. A comparison of World Health Organization tumor grades at recurrence in patients with non-skull base and skull base meningiomas. J Neurosurg. 2010;112(5):925–33.
12. Guevara P, Escobar-Arriaga E, Saavedra-Perez D, Martinez-Rumayor A, Flores-Estrada D, Rembao D, et al. Angiogenesis and expression of estrogen and progesterone receptors as predictive factors for recurrence of meningioma. J Neurooncol. 2010;98(3): 379–84.
13. Matsuno A, Fujimaki T, Sasaki T, Nagashima T, Ide T, Asai A, et al. Clinical and histopathological analysis of proliferative potentials of recurrent and non-recurrent meningiomas. Acta Neuropathol. 1996;91(5):504–10.
14. Takeuchi H, Kubota T, Kabuto M, Kitai R, Nozaki J, Yamashita J. Prediction of recurrence in histologically benign meningiomas: proliferating cell nuclear antigen and Ki-67 immunohistochemical study. Surg Neurol. 1997;48(5):501–6.
15. Lanzafame S, Torrisi A, Barbagallo G, Emmanuele C, Alberio N, Albanese V. Correlation between histological grade, MIB-1, p53, and recurrence in 69 completely resected primary intracranial meningiomas with a 6 year mean follow-up. Pathol Res Pract. 2000;196(7):483–8.
16. Adegbite AB, Khan MI, Paine KW, Tan LK. The recurrence of intracranial meningiomas after surgical treatment. J Neurosurg. 1983;58(1):51–6.
17. Mirimanoff RO, Dosoretz DE, Linggood RM, Ojemann RG, Martuza RL. Meningioma: analysis of recurrence and progression following neurosurgical resection. J Neurosurg. 1985;62(1): 18–24.
18. Ribom D, Eriksson A, Hartman M, Engler H, Nilsson A, Langstrom B, et al. Positron emission tomography (11)C-methionine and survival in patients with low-grade gliomas. Cancer. 2001; 92(6):1541–9.
19. Torii K, Tsuyuguchi N, Kawabe J, Sunada I, Hara M, Shiomi S. Correlation of amino-acid uptake using methionine PET and histological classifications in various gliomas. Ann Nucl Med. 2005;19(8):677–83.
20. Kim S, Chung JK, Im SH, Jeong JM, Lee DS, Kim DG, et al. 11C-methionine PET as a prognostic marker in patients with glioma: comparison with 18F-FDG PET. Eur J Nucl Med Mol Imaging. 2005;32(1):52–9.
21. Kato T, Shinoda J, Oka N, Miwa K, Nakayama N, Yano H, et al. Analysis of 11C-methionine uptake in low-grade gliomas and correlation with proliferative activity. AJNR Am J Neuroradiol. 2008;29(10):1867–71.
22. Lee JW, Kang KW, Park SH, Lee SM, Paeng JC, Chung JK, et al. 18F-FDG PET in the assessment of tumor grade and prediction of tumor recurrence in intracranial meningioma. Eur J Nucl Med Mol Imaging. 2009;36(10):1574–82.
23. Lippitz B, Cremerius U, Mayfrank L, Bertalanffy H, Raoofi R, Weis J, et al. PET-study of intracranial meningiomas: correlation with histopathology, cellularity and proliferation rate. Acta Neurochirurgica Suppl. 1996;65:108–11.
24. Tsuyuguchi N. Kinetic analysis of glucose metabolism by FDG-PET versus proliferation index of Ki-67 in meningiomas–comparison with gliomas. Osaka City Med J. 1997;43(2):209–23.
25. Cremerius U, Bares R, Weis J, Sabri O, Mull M, Schroder JM, et al. Fasting improves discrimination of grade 1 and atypical or malignant meningioma in FDG-PET. J Nucl Med. 1997; 38(1):26–30.
26. Iuchi T, Iwadate Y, Namba H, Osato K, Saeki N, Yamaura A, et al. Glucose and methionine uptake and proliferative activity in meningiomas. Neurol Res. 1999;21(7):640–4.
27. Gudjonsson O, Blomquist E, Lilja A, Ericson H, Bergstrom M, Nyberg G. Evaluation of the effect of high-energy proton irradiation treatment on meningiomas by means of 11C-L-methionine PET. Eur J Nucl Med. 2000;27(12):1793–9.
28. Okubo S, Zhen HN, Kawai N, Nishiyama Y, Haba R, Tamiya T. Correlation of L-methyl-11C-methionine (MET) uptake with L-type amino acid transporter 1 in human gliomas. J Neurooncol. 2010;99(2):217–25.
29. Kracht LW, Friese M, Herholz K, Schroeder R, Bauer B, Jacobs A, et al. Methyl-[11C]- L-methionine uptake as measured by positron emission tomography correlates to microvessel density in patients with glioma. Eur J Nucl Med Mol Imaging. 2003;30(6):868–73.
30. Arita H, Kinoshita M, Okita Y, Hirayama R, Watabe T, Ishohashi K, et al. Clinical characteristics of meningiomas assessed by ^{11}C-methionine and ^{18}F-fluorodeoxyglucose positron-emission tomography. J Neurooncol. 2012;107(2):379–86.
31. Abe Y, Matsuzawa T, Itoh M, Ishiwata K, Fujiwara T, Sato T, et al. Regional coupling of blood flow and methionine uptake in an experimental tumor assessed with autoradiography. Eur J Nucl Med. 1988;14(7–8):388–92.
32. Kimura H, Takeuchi H, Koshimoto Y, Arishima H, Uematsu H, Kawamura Y, et al. Perfusion imaging of meningioma by using continuous arterial spin-labeling: comparison with dynamic susceptibility-weighted contrast-enhanced MR images and histopathologic features. AJNR Am J Neuroradiol. 2006;27(1):85–93.
33. Siegers HP, Zuber P, Hamou MF, van Melle GD, de Tribolet N. The implications of the heterogeneous distribution of Ki-67 labelled cells in meningiomas. Br J Neurosurg. 1989;3(1):101–7.
34. Abramovich CM, Prayson RA. Histopathologic features and MIB-1 labeling indices in recurrent and nonrecurrent meningiomas. Arch Pathol Lab Med. 1999;123(9):793–800.
35. Bruna J, Brell M, Ferrer I, Gimenez-Bonafe P, Tortosa A. Ki-67 proliferative index predicts clinical outcome in patients with atypical or anaplastic meningioma. Neuropathology. 2007;27(2): 114–20.
36. Kim YJ, Ketter R, Henn W, Zang KD, Steudel WI, Feiden W. Histopathologic indicators of recurrence in meningiomas: correlation with clinical and genetic parameters. Virchows Archiv. 2006;449(5):529–38.
37. Moller ML, Braendstrup O. No prediction of recurrence of meningiomas by PCNA and Ki-67 immunohistochemistry. J Neurooncol. 1997;34(3):241–6.
38. Nakaguchi H, Fujimaki T, Matsuno A, Matsuura R, Asai A, Suzuki I, et al. Postoperative residual tumor growth of meningioma can be predicted by MIB-1 immunohistochemistry. Cancer. 1999;85(10):2249–54.
39. Abramovich CM, Prayson RA. MIB-1 labeling indices in benign, aggressive, and malignant meningiomas: a study of 90 tumors. Hum Pathol. 1998;29(12):1420–7.
40. Kolles H, Niedermayer I, Schmitt C, Henn W, Feld R, Steudel WI, et al. Triple approach for diagnosis and grading of meningiomas: histology, morphometry of Ki-67/Feulgen stainings, and cytogenetics. Acta Neurochir. 1995;137(3–4):174–81.
41. Langford LA, Cooksley CS, DeMonte F. Comparison of MIB-1 (Ki-67) antigen and bromodeoxyuridine proliferation indices in meningiomas. Hum Pathol. 1996;27(4):350–4.

MOLECULAR IMAGING AND BIOLOGY

Mol Imaging Biol (2014) 16:127–135
DOI: 10.1007/s11307-013-0670-7

Published Online: 20 July 2013

World Molecular Imaging Society

RESEARCH ARTICLE

Standardized Uptake Value in High Uptake Area on Positron Emission Tomography with ^{18}F-FRP170 as a Hypoxic Cell Tracer Correlates with Intratumoral Oxygen Pressure in Glioblastoma

Takaaki Beppu,[1] Kazunori Terasaki,[2] Toshiaki Sasaki,[2] Shunrou Fujiwara,[1] Hideki Matsuura,[1] Kuniaki Ogasawara,[1] Koichiro Sera,[2] Noriyuki Yamada,[3] Noriyuki Uesugi,[3] Tamotsu Sugai,[3] Kohsuke Kudo,[4] Makoto Sasaki,[4] Shigeru Ehara,[5] Ren Iwata,[6] Yoshihiro Takai[7]

[1]*Department of Neurosurgery, Iwate Medical University, Uchimaru 19-1, Morioka 020-8505, Japan*
[2]*Cyclotron Research Center, Iwate Medical University, Morioka, Japan*
[3]*Department of Clinical Pathology, Iwate Medical University, Morioka, Japan*
[4]*Institute for Biomedical Sciences, Iwate Medical University, Morioka, Japan*
[5]*Department of Radiology, Iwate Medical University, Morioka, Japan*
[6]*Cyclotron and Radioisotope Center (CYRIC), Tohoku University, Sendai, Japan*
[7]*Department of Radiology and Radiation Oncology, Hirosaki University Graduate School of Medicine, Hirosaki, Japan*

Abstract

Purpose: The aim of this study was to clarify the reliability of positron emission tomography (PET) using a new hypoxic cell tracer, 1-(2-[^{18}F]fluoro-1-[hydroxymethyl]ethoxy)methyl-2-nitroimidazole (^{18}F-FRP170).

Procedures: Twelve patients with glioblastoma underwent ^{18}F-FRP170 PET before tumor resection. Mean standardized uptake value (SUV) and normalized SUV were calculated at regions within a tumor showing high (high-uptake area) and relatively low (low-uptake area) accumulations of ^{18}F-FRP170. In these areas, intratumoral oxygen pressure (tpO_2) was measured using microelectrodes during tumor resection.

Results: Mean tpO_2 was significantly lower in the high-uptake area than in the low-uptake area. A significant negative correlation was evident between normalized SUV and tpO_2 in the high-uptake area.

Conclusion: The present findings suggest that high accumulation on ^{18}F-FRP170 PET represents viable hypoxic tissues in glioblastoma.

Key words: F-FRP170, PET, Hypoxia, Glioblastoma, Oxygen pressure, HIF1-α

Abbreviation: Cu-ATSM, ^{64}Cu-diacetyl-bis(N4-methylthiosemicarbazone); ^{18}F-FRP170, 1-(2-[^{18}F]fluoro-1-[hydroxymethyl]ethoxy)methyl-2-nitroimidazole; ^{18}F-FAZA, 1-α-D-(5-deoxy-5-[^{18}F]-fluoroarabinofuranosyl)-2-nitroimidazole; ^{18}F-FMISO, [^{18}F]fluoromisonidazole; Gd-T1WI, Gadolinium-enhanced T1-weighted imaging; HIF, Hypoxic-inducible factor; MRI, Magnetic resonance imaging; ROI, Region of interest; T2WI, T2-weighted imaging; PET, Positron emission tomography; VEGF, Vascular endothelial growth factor

Correspondence to: Takaaki Beppu; *e-mail:* tbeppu@iwate-med.ac.jp

Introduction

Almost all malignant solid tumors include hypoxic cells due to both excessive consumption and insufficient supply of oxygen within the tumor. Intratumoral hypoxia induces various biological characteristics in tumors. For instance, hypoxia in tumor activates the hypoxia-responsive elements such as hypoxia-inducible factors (HIFs), leading to transcription of target genes including vascular endothelial growth factor (VEGF). VEGF induces angiogenesis, and is also closely related to the proliferation and invasion of tumor. Gene instability caused by hypoxia must affect the differentiation of tumor cells. Intratumoral hypoxic conditions are disadvantageous in term of the production of peroxide radicals, which induces DNA damage under irradiation. Cancer stem cells existing within hypoxic tumor tissue have also been considered to represent a likely cause of radioresistance [1–3]. In glioblastoma, hypoxic conditions play a key role in the development of tumor characteristics. Neuroimaging enabling minimally invasive, objective, and quantitative evaluation of hypoxic conditions in glioblastoma would offer many clinical benefits in terms of diagnosis, selection of treatment, and prediction of prognosis.

Positron emission tomography (PET) using hypoxic cell tracers offers an attractive method for detecting hypoxic cells because it is simple, low-invasive, repeatable, and not limited in applicability to superficial tumors [4]. So far, hypoxic cells in brain tumors have been detected using PET with hypoxic cell tracers such as [^{18}F]fluoromisonidazole (^{18}F-FMISO) [5–7], 1-α-D-(5-deoxy-5-5-[^{18}F]-fluoroarabinofuranosyl)-2-nitroimidazole (^{18}F-FAZA) [8], and ^{64}Cu-diacetyl-bis(N4-methylthiosemicarbazone) (Cu-ATSM) [9, 10]. A new hypoxic cell tracer, 1-(2-[^{18}F]fluoro-1-[hydroxymethyl]ethoxy)methyl-2-nitroimidazole (^{18}F-FRP170), has recently been identified [11, 12]. PET using ^{18}F-FRP170 (^{18}F-FRP170 PET) has already been performed for detecting hypoxic cells in malignant brain tumors, and the potential of this new tracer has been documented [13]. Several studies assessing intratumoral oxygen condition using electrodes or other methods have confirmed reliability of PET with various hypoxic cell tracers other than ^{18}F-FRP170 [14–17]. However, whether areas of high accumulation on ^{18}F-FRP170 PET really represent tissues including hypoxic cells, and to what degree areas of high accumulation represent regions under hypoxic conditions have remained unclear. The aim of this study was to confirm the reliability of ^{18}F-FRP170 PET for detecting hypoxic cells. We therefore compared standardized uptake value (SUV) measured on ^{18}F-FRP170 PET with intratumoral oxygen pressure (tpO_2) within glioblastoma measured using oxygen microelectrodes during tumor resection. Furthermore, we performed immunohistochemical detection HIF-1, a heterodimeric nuclear transcription factor playing a critical role in cellular response to low oxygen pressure [18], in tissues corresponding to the regions of interest (ROIs) on ^{18}F-FRP170 PET images.

Materials and Methods

Patients

All study protocols were approved by the Ethics Committee of Iwate Medical University, Morioka, Japan (No. H22-70). Patients recruited to this study were admitted to Iwate Medical University Hospital between April 2008 and December 2012. Entry criteria for the study were: patients ≥20 years old with non-treated glioblastoma localized in cerebral white matter other than the brain stem or cerebellum, performance of ^{18}F-FRP170 PET and measurement of absolute oxygen pressure within the tumor according to the study protocol, and voluntary provision of written informed consent to participate. Preoperative diagnosis was based on present history and findings from conventional magnetic resonance imaging (MRI) on admission, and final diagnosis of glioblastoma was made based on histological features after surgery. Twelve patients (ten men, two women, mean age, 63±13.7 years) were enrolled after excluding patients who did not meet the entry criteria (Table 1).

^{18}F-FRP170 PET

Within 7 days (mean, 4.3±2.4 days) before surgery for tumor resection, both conventional MRI including gadolinium-enhanced T1-weighted imaging (Gd-T1WI) and ^{18}F-FRP170 PET were performed. The ^{18}F-FRP170 was synthesized using on-column alkaline hydrolysis according to the methods described by Ishikawa et al. [12]. The final formulation for injection was formed in normal saline containing 2.5 %*v*/*v* ethanol using solid-phase extraction techniques. At 60 min after intravenous injection of approximately 370 MBq (mean, 5.9±1.8 MBq/kg) of ^{18}F-FRP170, PET was performed using a PET/computed tomography (CT) system (SET3000 GCT/M; Shimazu, Japan). On ^{18}F-FRP170 PET, ROIs of 10 mm in diameter were placed at areas of high accumulation (high-uptake area) and relatively low accumulation (low-uptake area) within the tumor bulk (Fig. 1a, b). These ROIs were placed at regions as close to the brain surface as possible to allow easy and safe insertion of microelectrodes for measuring oxygen pressure during surgery. A ROI was also placed in apparent normal cerebral white matter of the contralateral side. SUV for each ROI was automatically determined. Although both mean and maximal values of SUV in ROI were measured, we defined the mean value of SUV as "SUV" in this study. The normalized SUV, defined as SUV for each high- or low-uptake area divided by SUV for the apparent normal cerebral white matter of the contralateral hemisphere, was also calculated.

Immediately before surgery for each patient, we created a fusion image that combined a three-dimensional ^{18}F-FRP170 PET image with Gd-T1WI using a surgical navigation system (Stealth Station TRIA plus; Medtronics, Minneapolis, MN) in the operation room. On the fusion image, both high- and low-uptake areas were identified stereotactically for each patient (Fig. 2a–d).

Measurement of Intratumoral Oxygen Pressure During Surgery

Measurement of tpO_2 was performed during surgery for aggressive tumor resection. The tpO_2 level was measured using disposable

Table 1. Patient characteristics and measurement data

No.	Sex	Age (year)	Location	SUV			Normalized SUV		tpO_2 (mmHg)		PaO_2 (mmHg)	HIF-1α staining
				High uptake	Low uptake	ANWM	High uptake	Low uptake	High uptake	Low uptake		
1	M	76	Parietal lobe	0.99	0.54	0.54	1.83	1.00	23	44	157	–
2	M	81	Parietal lobe	2.22	1.39	1.04	2.13	1.34	16	45	128	–
3	M	59	Frontal lobe	1.46	1.16	0.87	1.69	1.33	28	56	176	–
4	F	61	Frontal lobe	1.10	0.87	0.74	1.49	1.18	32	54	145	–
5	M	75	Parietal lobe	1.83	1.11	0.83	2.20	1.34	16	33	143	–
6	F	54	Parietal lobe	1.43	0.82	0.62	2.31	1.32	30	54	134	–
7	M	64	Temporal lobe	1.62	1.00	0.72	2.25	1.39	15	27	158	+
8	M	54	Occipital lobe	1.50	1.01	0.76	1.97	1.33	17	35	120	+
9	M	67	Frontal lobe	1.84	1.46	1.13	1.63	1.29	25	36	132	+
10	M	76	Temporal lobe	1.90	0.92	0.77	2.47	1.19	15	26	124	+
11	M	58	Frontal lobe	1.37	1.25	0.90	1.52	1.39	24	34	137	+
12	M	31	Frontal lobe	1.66	1.11	0.87	1.91	1.28	20	37	148	+

ANWM apparent normal white matter, *tpO2* intratumoral oxygen pressure

Clark-type electrodes (UOE-04TS; Unique Medical, Tokyo, Japan) at the tip of a sensor (Teflon-coated tube; diameter, 0.4 mm; length, 10 mm). Immediately before surgery, electrodes were sterilized by immersion in a solution of 2.25*w/v*% glutaraldehyde and buffer for 2 h, then washed with sterilized physiological saline solution. The electrode was then connected to a digital oxygen pressure monitor (POG-203; Unique Medical) to calibrate the value of oxygen pressure to 150 mmHg in a sterilized physiological saline solution prior to insertion into the tumor. After craniotomy, we stereotactically inserted a needle-shaped navigating marker of 2 mm in diameter into the center region of the high-uptake area where the ROI had been placed before surgery through the dura mater, while we observed the localization of the tip of the marker in the tumor on the monitor of the surgical navigation system (Fig. 2c, d). After removal of the navigation marker, we immediately inserted the electrode along the same trajectory through the dura mater, with the tip of the electrode placed within tumor tissue of the high-uptake area. A digital monitor was then used to measure tpO_2. We observed tpO_2 value gradually declined from 150 mmHg while rising and falling on the digital monitor, and defined the minimum value as the absolute tpO_2 value at the high-uptake area for each patient. After completely washing and calibrating the value of oxygen pressure to 150 mmHg in a sterilized physiological saline solution, the same procedure described above was performed to measure tpO_2 in the low-uptake area. During measurements of tpO_2, arterial oxygen pressure (PaO_2) was measured using arterial blood obtained from the radial artery. After measuring tpO_2 and removing the electrode, we inserted a needle for biopsy along a trajectory to obtain tumor tissues from the high- and low-uptake areas in six patients. In all cases, the tumor was successfully removed after completing the procedures described above.

HIF-1α Immunohistochemistry

Immunohistochemical staining of HIF-1α was performed on specimens obtained from tumor resection for six patients. From all specimens in both high- and low-uptake areas, paraffin-embedded tissue sections of 3-μm-thickness were collected onto 3-aminoprophyltriethoxylane-coated glass slides. The dewaxed preparations were given microwave pretreatment for 30 min in sodium citrate. The preparations were incubated for 60 min using rabbit anti-HIF-1α monoclonal antibody (clone, H1alpha67; Novus Biologicals, Littleton, CO) at 1:200 dilution. Preparations were incubated using peroxidase-based EnVision kits (Dako Japan, Tokyo, Japan) as the secondary antibody, then immersed in diaminobenzidine/H_2O_2 solution for colored visualization. Finally, preparations were counterstained with hematoxylin.

We observed the staining attitude of HIF-1α in tumor cells for all patients. We also evaluated the HIF-1α staining indices for each high- or low-uptake area for each patient, defined as the percentage of cells showing nuclear staining as determined by counting approximately 1,000 cells under light microscopy (×400 magnification).

Statistical Analyses

In all patients, differences in SUV, normalized SUV, and HIF-1α staining index were compared between high- and low-uptake areas using the Mann–Whitney *U* test. Differences in intratumoral pO_2 between high- and low-uptake areas were also compared in all patients using the Mann–Whitney *U* test. Correlations between PaO_2 and tpO_2 and between normalized SUV and tpO_2 for all patients were analyzed in each high- and low-uptake area using Pearson's correlation coefficient test.

Results

Scanning at 60 min after intravenous injection of tracer provided fine contrast images that enabled visual differentiation between high- and low-uptake areas in all patients. In eight patients with glioblastoma presenting a central necrotic region, ^{18}F-FRP170 was partially accumulated in the intermediate layer between the deep layer surrounding the central necrotic region and the outer layer within the peripheral region of tumor involved in lesion enhancement on Gd-T1WI (Fig. 1a, b). Fusion images combining Gd-T1WI and ^{18}F-FRP170 PET provided precise locations of both high- and low-uptake regions during surgery, and allowed us to successfully insert electrodes and obtain the

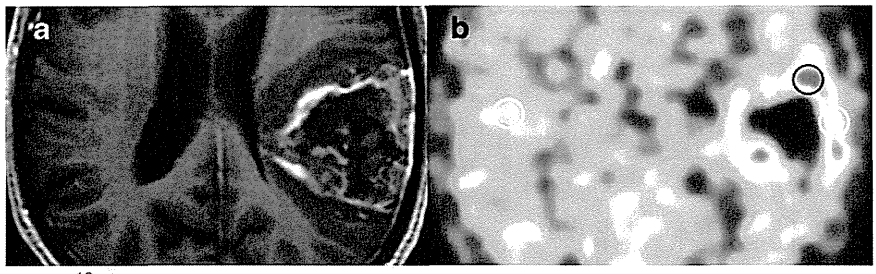

Fig. 1. Typical findings of ^{18}F-FRP170 PET in glioblastoma with a large area of central necrosis in Case 1. High-uptake areas are seen partially in the area between the outer peripheral region showing enhancement on Gd-T1WI and a deeper region adjacent to the central necrotic region. ROIs were placed on a high-uptake area (*black circle*) and a relatively low-uptake area (*white circle*) within the tumor bulk showing enhancement on Gd-T1W, and also on apparent normal white matter of the contralateral hemisphere (*white circle*). **a** Gd-T1WI, **b** ^{18}F-FRP170 PET.

sampling tissues (Fig. 2a–d). No patient presented with any complications due to ^{18}F-FRP170 PET.

Mean SUV for high-uptake areas, low-uptake areas, and contralateral normal white matter regions were 1.58±0.35, 1.05±0.25, and 0.82±0.16, respectively. Significant differences in mean SUV were found between high- and low-uptake areas (p=0.001), between high-uptake areas and normal white matter (p<0.001), and between low-uptake areas and normal white matter (p=0.01), although SUV values in the three groups overlapped (Fig. 3a). Mean normalized SUV for the high- and low-uptake areas were calculated as 1.95±0.33 and 1.28±0.11, respectively. Mean normalized SUV for the high-uptake area differed significantly (p<0.001) and clearly from that of the low-uptake area, with a cut-off level of around 1.4 (Fig. 3b). Mean tpO_2 was significantly lower in high-uptake areas (21.7±

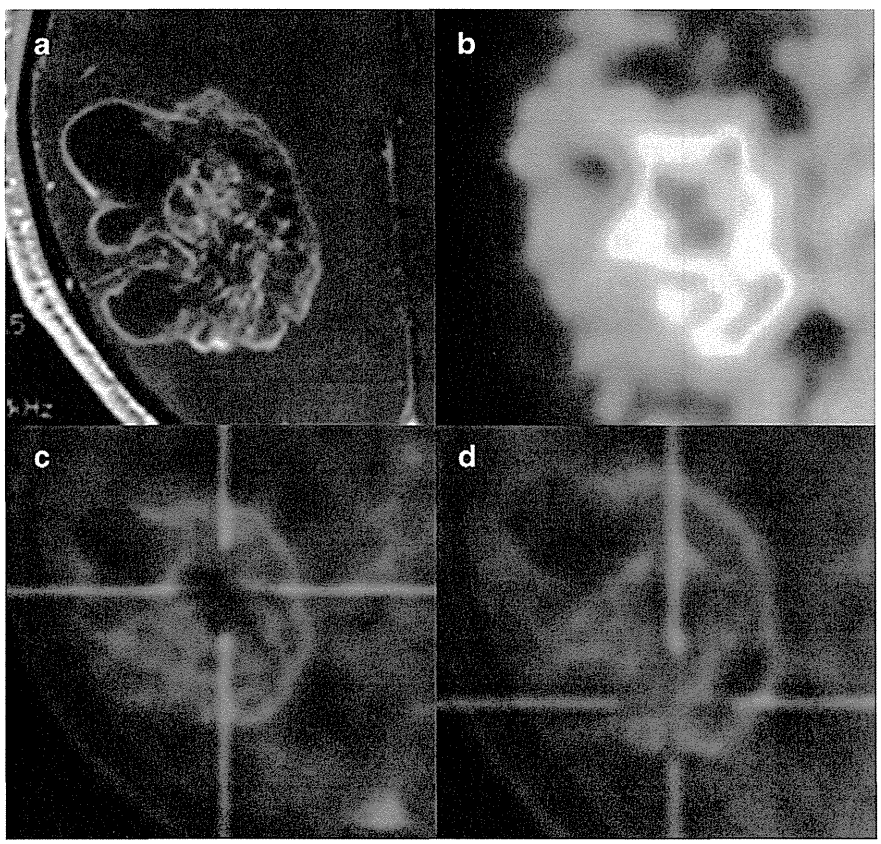

Fig. 2. High- and low-uptake areas were stereotactically localized on fusion images combining Gd-T1WI (**a**) and ^{18}F-FRP170 PET (**b**) for Case 5, to identify tumor tissues corresponding to ROIs. On fusion images, high- and low-uptake areas were depicted as bluish regions (**c**) and greenish regions (**d**), respectively.

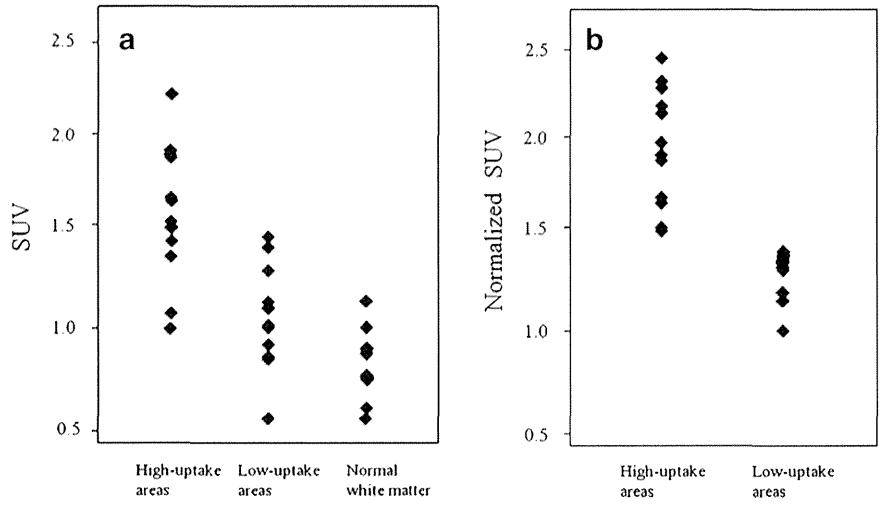

Fig. 3. **a** Differences in SUV among the high-uptake area, low-uptake area, and apparent normal white matter. **b** Difference in normalized SUV between high- and low-uptake areas.

6.2 mmHg) than in low-uptake areas (40.1±10.4 mmHg; $p<0.001$, Fig. 4). In terms of the relationship between normalized SUV and tpO_2 in all patients, a significant negative correlation was found in high-uptake areas ($r=-0.64$, $p=0.03$), whereas no significant correlation was identified in low-uptake areas (Fig. 5a, b). No significant correlations between PaO_2 and tpO_2 were found in either high- or low-uptake areas (not shown).

On specimens obtained from high-uptake areas, HIF-1α was clearly detectable in nuclei in all six patients, with three patients also showing HIF-1α staining in cytoplasm. On the other hand,

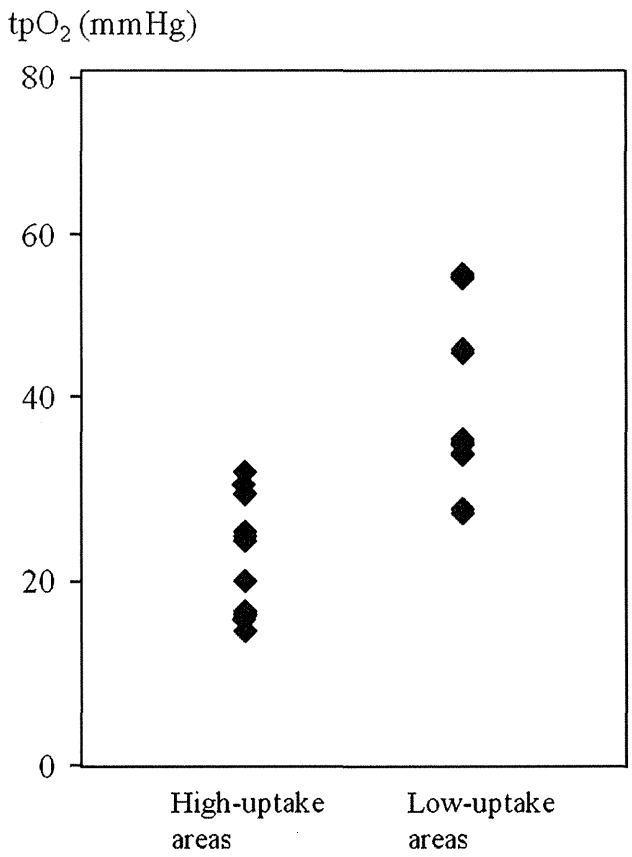

Fig. 4. Difference in tpO_2 between high- and low-uptake areas.

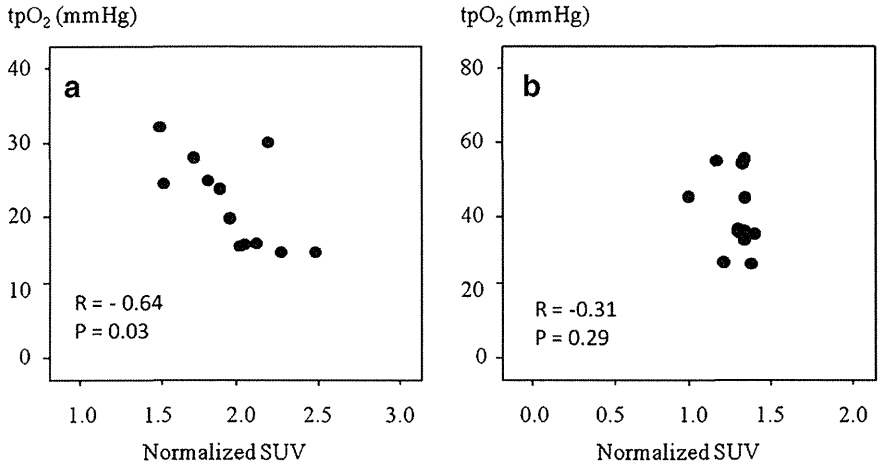

Fig. 5. Correlations between normalized SUV and tpO_2 in high-uptake areas (**a**) and low-uptake areas (**b**).

specimens from low-uptake areas showed three different patterns, with HIF-1α staining only cytoplasm in three patients, and both nuclei and cytoplasm in two patients. In the remaining patient, few barely surviving cells with HIF-1α staining were seen within a wide area of necrotic tissue (Fig. 6a–d). HIF-1α staining indices ranged from 35.2 to 63.5 % in high-uptake areas, and from 8.9 to 35.9 % in low-uptake areas. Mean HIF-1α staining index was significantly higher in high-uptake areas (mean, 53.0±10.2 %) than in low-uptake areas (mean, 18.9± 9.5 %). Notably, HIF-1α staining index was markedly low (8.9 %) in necrotic tissue obtained from a low-uptake area in one patient.

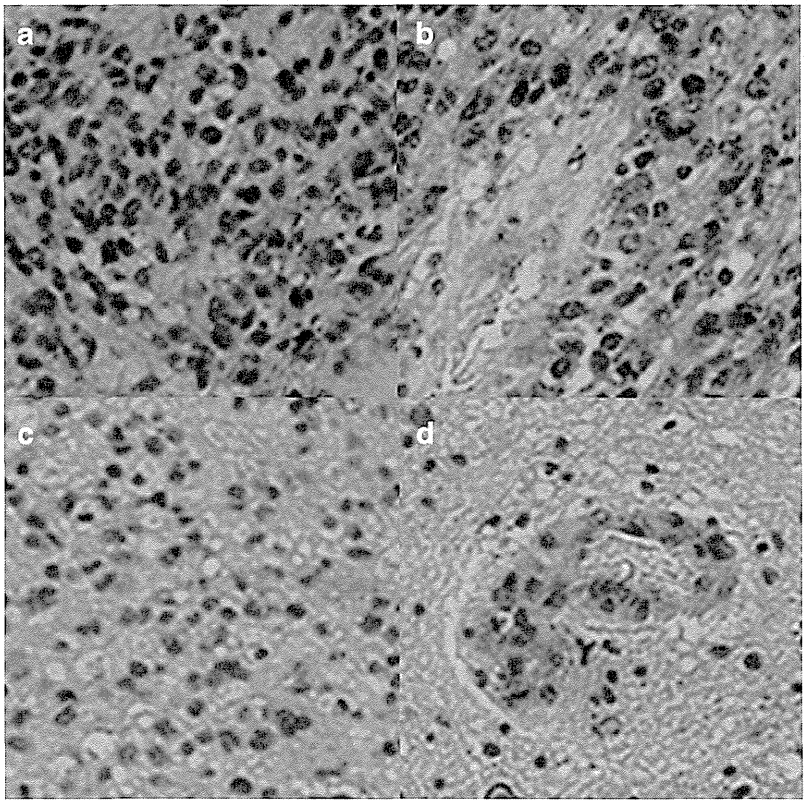

Fig. 6. Findings for HIF-1α immunostaining of tissues from high-uptake areas (**a**, **b**) and low-uptake areas (**c**, **d**). **a** HIF-1α was strongly detected in nuclei in all patients. **b** HIF-1α was stained in both cytoplasms and nuclei in three patients. **c** HIF-1α was stained only in cytoplasm in three patients. **d** A few HIF-1α-stained cells were seen within a wide necrotic tissue in one patient.

Discussion

The present study showed that mean values of both SUV and normalized SUV were significantly higher in high-uptake areas than in low-uptake areas. In particular, normalized SUV values in high-uptake areas were absolutely higher than those in low-uptake areas. In this study, approximately 370 MBq of ^{18}F-FRP170 was administered intravenously for all patients, according to a report by Shibahara et al. [13]. Absolute SUV might thus have been subtly influenced by the delivered volume of tracer into the tumor as determined by individual parameters, such as body size, cardiac output volume, and blood pressure. As normalization of absolute SUV can eliminate differences in these factors, we emphasize the importance of estimation using normalized SUV. In the present study, tpO_2 did not correlate with PaO_2 at all. Two previous reports examining both tpO_2 in brain tumors and PaO_2 could not find any relationship between these measured values, although correlations were not estimated statistically [19, 20]. Our results support those previous reports and indicate that tpO_2 was not influenced by PaO_2 during surgery. Values of tpO_2 were significantly lower in high-uptake areas (21.7± 6.2 mmHg) than in low-uptake areas (40.1±10.4 mmHg). Furthermore, a significant correlation was found between normalized SUV and tpO_2 in high-uptake areas. These results indicate that high-uptake areas where ^{18}F-FRP170 accumulates show relatively more hypoxic conditions than low-uptake areas, suggesting the reliability of findings from ^{18}F-FRP170 PET.

Selective accumulation of ^{8}F-FRP170 in hypoxic cells has been considered to proceed as follows. First, the nitroimidazole moiety in ^{18}F-FRP170 is responsible for the initial accumulation in hypoxic cells. After passive diffusion inside the cells, enzymatic nitroreduction by nitroreductase results in nitroimidazole changing to radical anions. Under normoxic conditions, these radical anions are reoxidized and diffuse out of the cells, whereas products comprising radical anions covalently bound to intracellular macromolecules are trapped within cells under hypoxic conditions [13, 21–23]. As a result, ^{18}F-FRP170 can accumulate only within viable and active hypoxic cells, but cannot accumulate within normoxic cells or even hypoxic cells with low metabolism such as apoptotic or necrotic cells. A previous report assessing accumulation of ^{18}F-FRP170 in a rat model of ischemic myocardium using autoradiography documented that ^{18}F-FRP170 was observed only within viable hypoxic myocardiac cells [11]. As absolute SUV must correlate with the concentration of PET tracer within the tissue, SUV on ^{18}F-FRP170 PET should increase with a higher density of viable hypoxic cells within the tissues of the ROI. We think that such high-uptake areas represent glioblastoma tissue comprising a high density of viable hypoxic cells. In contrast, tissues of low-uptake areas might represent low densities of viable hypoxic cells. In other words, a majority of cells in low-uptake areas could not accumulate ^{18}F-FRP170 because of the presence of either viable cells containing relatively higher tpO_2 than high-uptake area or low metabolic-hypoxic cells degenerating in apoptosis or necrosis. The oxygen environment may thus differ substantially among different regions in low-uptake areas, despite the similar content of viable hypoxic cells. Indeed, tpO_2 levels showed a wide range in low-uptake areas, with a large standard deviation (Fig. 4). This might be one reason for the lack of significant correlation between tpO_2 levels and normalized SUV in low-uptake areas. As intratumoral hypoxia is generally considered to result from insufficient oxygen supply paralleling the distance from normal vessels surrounding the tumor, intratumoral oxygen pressure should be higher in more peripheral regions of glioblastoma that are also supplied with blood from normal vessels surrounding the tumor bulk [24, 25]. On PET in the present study, interestingly, high-uptake areas were observed partially within the intermediate layer of enhancing lesions on Gd-T1WI, and low-uptake areas were seen not only in the peripheral layer external to the intermediate layer containing high-uptake areas but also in the inner core layer adjacent to the central necrosis deep to the intermediate layer (Fig. 1b). We assumed that low-uptake areas in both peripheral and inner core layers might contain little ^{18}F-FRP170-accumulating hypoxic cells, but the peripheral layers included many viable cells at relatively high oxygen pressure, while the inner core comprises low metabolic-hypoxic cells undergoing degenerative apoptosis or necrosis. Remaining low-uptake areas in the intermediate layer probably represent mixture of the two histological types described above. Pistollato et al. [26] evaluated biological characteristics in tissues isolated from three concentric layers (core, intermediate, and peripheral layers) in glioblastoma. The core and intermediate layers showed expression of HIF-1α as a hypoxic cell marker, whereas the peripheral layer did not express HIF-1α, but showed expressions of glial fibrillary acidic protein and β-III-tubulin as mature neural cell markers. In addition, core and intermediate layers contained more glioblastoma stem cells, which are well known to be frequently seen in hypoxic niches. These results suggest that inner core and peripheral layers depicted as low-uptake areas on ^{18}F-FRP170 PET in the present study are likely to exhibit hypoxic and relatively normoxic conditions, respectively.

Hypoxic condition rapidly induces overexpression of HIF-1α for transcripting target genes such as vascular endothelial growth factor to induce angiogenesis, as countermeasures against hypoxic conditions. Under normoxic conditions, prolyl hydroxylation is induced in HIF-1α, allowing binding to the von-Hipple-Lindau protein, which mediates ubiquitination of HIF-1α and subsequent proteasomal degeneration in the cytoplasm. However, under hypoxic conditions, the oxygen requiring prolyl hydroxylase remains inactive, resulting in accumulation of the constitutively expressed HIF-1α protein in cytoplasm. This subunit is phosphorylated and translocated to the nucleus, where it dimerizes with the HIF-1β subunit, binding to the hypoxia-

response elements upstream of HIF-1-regulated target genes [27]. Therefore, increasingly activated-HIF-1α induced by hypoxia accumulates in the nucleus. In this study, all specimens obtained from high-uptake areas clearly showed nuclear staining for HIF-1α, whereas this finding was seen in low-uptake areas in only two patients. Furthermore, mean HIF-1α staining index determined by the percentage of cells showing nuclear staining was significantly higher in high-uptake areas than in low-uptake areas. Necrotic tissue obtained from a low-uptake area of one patient showed an extremely low HIF-1α staining index. These findings might support the concept that high-uptake areas represent more hypoxic regions with a high density of viable and active hypoxic cells. Tissues of low-uptake areas were not obtained from deeper than high-uptake areas but rather from the same depth or more externally during surgery in all six patients. As a result, HIF-1α was also detected in the low-uptake areas of all patients, but showed a greater variety of features than high-uptake areas. These findings support the possibility that low-uptake areas comprised either numerous viable cells under conditions of relatively higher oxygen pressure or low metabolic hypoxic cells under degenerative apoptosis or necrosis.

In the present study, PET at 60 min after intravenous injection of ^{18}F-FRP170 could provide visually fine-contrast PET images. Shidehara et al. [13] reported fine-contrast color images provided by imaging at 120 min after injection of ^{18}F-FRP170 in patients with malignant brain tumor. Kaneta et al. [21] reported that imaging results at 120 min after injection of ^{18}F-FRP170 for patients with lung cancer contributed only a slightly higher tumor/blood ratio when compared with that at 60 min, and concluded that imaging at 60 min after administration was clinically sufficient for assessing hypoxic cells in tumors. The present study supported these recommendations by Kaneta et al. In an experimental study using mice bearing cultured cancer cells, ^{18}F-FAZA displayed significant higher tumor-to-background ratios compared with ^{18}F-FMISO and another azomycin-based nucleoside, iodoazomycin arabinoside, labeled with ^{124}I (^{124}I-IAZA), when scanning for all tracer was fixed in 3 h post-injection [28]. Clinically, PET imaging with ^{18}F-FMISO and ^{18}F-FAZA has usually been scanned at 120–140 [5–7] and 120–210 min [8] after administration, respectively. Although no previous reports have directly compared ^{18}F-FRP170 PET and ^{18}F-FMISO PET images, ^{18}F-FRP170 PET has been considered superior in terms of fine contrast and rapid clearance from blood [21]. The short duration for imaging could represent an additional advantage to ^{18}F-FRP170 PET.

Some limitations regarding the interpretation of study results must be considered for this study. First, the sample size in this study was small. Additional studies of a larger number of patients with glioblastoma are needed. Second, use of smaller ROIs might provide more rigorous results in comparisons among SUV, tpO_2, and histological features. However, in this study, we placed relatively huge ROIs of 10 mm in diameter to avoid misplacement of microelectrodes within the ROI and sampling error of tumor tissues corresponding to the ROI. These issues could represent factors contributing to make maximum SUV within the ROI unsuitable for use in this study. In short, errors involving differences between pinpoint regions for insertion of electrode and maximum SUV could easily anticipated. Third, direct tpO_2 measurements using microelectrodes available differ in sensitivity, accuracy, ability to measure oxygen availability among types of probe used, and impossibility in differentiation between hypoxic and necrotic tissues, although this technique is commonly considered a gold standard [4]. Other techniques indirectly measuring oxygen through reduced drug levels, hemoglobin saturation, or perfusion have been proposed. However, indirect measurements, although valuable, require a set of assumptions to relate the measurement to tpO_2 or oxygen concentration [4]. Fourth, measurement of tpO_2 using electrodes in this study did not strictly represent intracellular oxygen pressure, but rather the oxygen pressure of tissue containing hypoxic cells. However, tpO_2 as measured in this study would correlate with intracellular oxygen pressure, as intracellular oxygen pressure is regulated by extracellular conditions. Fifth, measured tpO_2 values in this study were relatively higher (21.7±6.2 mmHg in high-uptake areas and 40.1±10.4 mmHg in low-uptake areas) than in previous reports of direct measurement using Eppendorf oxygen electrodes in malignant brain tumors, where mean tpO_2 has been reported as approximately ≤20 mmHg [20, 24, 29]. In particular, mean value in low-uptake areas was significantly higher. However, mean tpO_2 in low-uptake areas was lower that of brain tissue around the tumor (59.8±6.5 mmHg) in a previous report [20]. In previous reports regarding oxygen pressure at high-uptake areas on ^{18}F-FMISO PET in animal tumor models, measurements using Eppendorf electrodes showed a high frequency of tpO_2 ≤10 mmHg [15, 30, 31]. Although the reasons for this contradiction are not entirely clear, we consider these results may have arisen from differences in the electrodes used, or from the inflow of a small amount of air into the trajectory when electrodes were inserted immediately after removal of the navigation marker with a larger diameter than the electrode. However, as this issue applied to measurements of tpO_2 for all patients in this study, the findings of higher tpO_2 in high-uptake areas compared to low-uptake areas appear valid.

Conclusions

Findings of a significant correlation between normalized SUV and tpO_2, and strong nuclear immunostaining for HIF-1α in areas of high ^{18}F-FRP170 accumulation, suggest that high-uptake areas on ^{18}F-FRP170 PET represent high densities of viable hypoxic cells, at least in glioblastoma. However, interpretation of low-uptake areas is more complicated, given the likelihood that these lesions comprise

various oxygen environments containing low densities of viable hypoxic cells.

Acknowledgments. This study was supported in part by Grant-in-Aid for Strategic Medical Science Research Center for Advanced Medical Science Research from the Ministry of Science, Education, Sports and Culture, Japan.

Conflict of Interest. The authors declare that they have no conflicts of interest.

References

1. Jensen RL (2009) Brain tumor hypoxia: tumorigenesis, angiogenesis, imaging, pseudoprogression, and as a therapeutic target. J Neurooncol 92:317–335
2. Jensen RL (2006) Hypoxia in the tumorigenesis of gliomas and as a potential target for therapeutic measures. Neurosurg Focus 20:E24
3. Rich JN (2007) Cancer stem cells in radiation resistance. Cancer Res 67:8980–8984
4. Mendichovszky I, Jackson A (2011) Imaging hypoxia in gliomas. Br J Radiol 84(2):S145–S158
5. Eschmann SM, Paulsen F, Reimold M et al (2005) Prognostic impact of hypoxia imaging with 18F-misonidazole PET in non-small cell lung cancer and head and neck cancer before radiotherapy. J Nucl Med 46:253–260
6. Kawai N, Maeda Y, Kudomi N et al (2011) Correlation of biological aggressiveness assessed by 11C-methionine PET and hypoxic burden assessed by 18F-fluoromisonidazole PET in newly diagnosed glioblastoma. Eur J Nucl Med Mol Imaging 38:441–450
7. Swanson KR, Chakraborty G, Wang CH et al (2009) Complementary but distinct roles for MRI and 18F-fluoromisonidazole PET in the assessment of human glioblastomas. J Nucl Med 50:36–44
8. Postema EJ, McEwan AJ, Riauka TA et al (2009) Initial results of hypoxia imaging using 1-alpha-D: -(5-deoxy-5-[^{18}F]-fluoroarabinofuranosyl)-2-nitroimidazole (^{18}F-FAZA). Eur J Nucl Med Mol Imaging 36:1565–1573
9. Sheehan JP, Popp B, Monteith S et al (2011) Trans sodium crocetinate: functional neuroimaging studies in a hypoxic brain tumor. J Neurosurg 115:749–753
10. Tateishi K, Tateishi U, Sato M et al (2013) Application of ^{62}Cu-diacetyl-bis (N4-methylthiosemicarbazone) PET imaging to predict highly malignant tumor grades and hypoxia-inducible factor-1alpha expression in patients with glioma. AJNR Am J Neuroradiol 34:92–99
11. Kaneta T, Takai Y, Kagaya Y et al (2002) Imaging of ischemic but viable myocardium using a new 18F-labeled 2-nitroimidazole analog, 18F–FRP170. J Nucl Med 43:109–116
12. Ishikawa Y, Iwata R, Furumoto S, Takai Y (2005) Automated preparation of hypoxic cell marker [^{18}F]FRP-170 by on-column hydrolysis. Appl Radiat Isot 62:705–710
13. Shibahara I, Kumabe T, Kanamori M et al (2010) Imaging of hypoxic lesions in patients with gliomas by using positron emission tomography with 1-(2-[^{18}F] fluoro-1-[hydroxymethyl]ethoxy)methyl-2-nitroimidazole, a new 18F-labeled 2-nitroimidazole analog. J Neurosurg 113:358–368
14. Matsumoto K, Szajek L, Krishna MC et al (2007) The influence of tumor oxygenation on hypoxia imaging in murine squamous cell carcinoma using [^{64}Cu]Cu-ATSM or [^{18}F]Fluoromisonidazole positron emission tomography. Int J Oncol 30:873–881
15. Sorensen M, Horsman MR, Cumming P et al (2005) Effect of intratumoral heterogeneity in oxygenation status on FMISO PET, autoradiography, and electrode Po2 measurements in murine tumors. Int J Radiat Oncol Biol Phys 62:854–861
16. Mahy P, De Bast M, Gallez B et al (2003) In vivo colocalization of 2-nitroimidazole EF5 fluorescence intensity and electron paramagnetic resonance oximetry in mouse tumors. Radiother Oncol 67:53–61
17. Tran LB, Bol A, Labar D et al (2012) Hypoxia imaging with the nitroimidazole ^{18}F-FAZA PET tracer: a comparison with OxyLite, EPR oximetry and 19F-MRI relaxometry. Radiother Oncol 105:29–35
18. Wang GL, Semenza GL (1995) Purification and characterization of hypoxia-inducible factor 1. J Biol Chem 270:1230–1237
19. Collingridge DR, Piepmeier JM, Rockwell S, Knisely JP (1999) Polarographic measurements of oxygen tension in human glioma and surrounding peritumoural brain tissue. Radiother Oncol 53:127–131
20. Kayama T, Yoshimoto T, Fujimoto S, Sakurai Y (1991) Intratumoral oxygen pressure in malignant brain tumor. J Neurosurg 74:55–59
21. Kaneta T, Takai Y, Iwata R et al (2007) Initial evaluation of dynamic human imaging using ^{18}F-FRP170 as a new PET tracer for imaging hypoxia. Ann Nucl Med 21:101–107
22. Chapman JD (1979) Hypoxic sensitizers—implications for radiation therapy. N Engl J Med 301:1429–1432
23. Krohn KA, Link JM, Mason RP (2008) Molecular imaging of hypoxia. J Nucl Med 49(Suppl 2):129S–148S
24. Beppu T, Kamada K, Yoshida Y et al (2002) Change of oxygen pressure in glioblastoma tissue under various conditions. J Neurooncol 58:47–52
25. Brown JM (1979) Evidence for acutely hypoxic cells in mouse tumours, and a possible mechanism of reoxygenation. Br J Radiol 52:650–656
26. Pistollato F, Abbadi S, Rampazzo E et al (2010) Intratumoral hypoxic gradient drives stem cells distribution and MGMT expression in glioblastoma. Stem Cells 28:851–862
27. Fischer I, Gagner JP, Law M, Newcomb EW, Zagzag D (2005) Angiogenesis in gliomas: biology and molecular pathophysiology. Brain Pathol 15:297–310
28. Reischl G, Dorow DS, Cullinane C et al (2007) Imaging of tumor hypoxia with [^{124}I]IAZA in comparison with [^{18}F]FMISO and [^{18}F]FAZA-first small animal PET results. J Pharm Pharm Sic 10:203–211
29. Rampling R, Cruickshank G, Lewis AD et al (1994) Direct measurement of pO2 distribution and bioreductive enzymes in human malignant brain tumors. Int J Radiat Oncol Biol Phys 29:427–431
30. Piert M, Machulla H, Becker G et al (1999) Introducing fluorine-18 fluoromisonidazole positron emission tomography for the localisation and quantification of pig liver hypoxia. Eur J Nucl Med 26:95–109
31. Bartlett RM, Beattie BJ, Naryanan M et al (2012) Image-guided PO2 probe measurements correlated with parametric images derived from ^{18}F-fluoromisonidazole small-animal PET data in rats. J Nucl Med 53:1608–1615

Neurol Med Chir (Tokyo) 53, 779–785, 2013

doi: 10.2176/nmc.oa2013-0211
Online October 21, 2013

Special Theme Topic:
Treatment of Malignant Brain Tumor

Retrospective Analysis of Bevacizumab in Combination with Ifosfamide, Carboplatin, and Etoposide in Patients with Second Recurrence of Glioblastoma

Yoshiki ARAKAWA,[1] Takashi MIZOWAKI,[2] Daiki MURATA,[1] Koichi FUJIMOTO,[1] Takayuki KIKUCHI,[1] Takeharu KUNIEDA,[1] Jun C. TAKAHASHI,[1] Yasushi TAKAGI,[1] and Susumu MIYAMOTO[1]

Departments of [1]Neurosurgery and [2]Radiation Oncology and Image-applied Therapy, Kyoto University Graduate School of Medicine, Kyoto, Kyoto

Abstract

Bevacizumab has been reported to be effective for recurrent glioblastoma. In our hospital, ifosfamide, carboplatin, etoposide (ICE) is the second-line chemotherapy for first recurrence of glioblastoma after temozolomide failure. In the present analysis, we retrospectively investigated the feasibility and effectiveness of bevacizumab combined with ICE in patients with glioblastoma at second relapse during ICE treatment. Between 2010 and 2012, tumor progressions were diagnosed in consecutive 8 patients who were treated with ICE for the first recurrence of glioblastoma. These patients were administered 3 cycles of 10 mg/kg bevacizumab every two weeks in combination with ICE treatment. The objective response rate of bevacizumab combination was 75% in Neuro-Oncology Working Group (RANO criteria), including complete response and partial response. Median progression free survival (PFS) and median overall survival (OS) after second relapse were 3.7 months (95% confidence interval [CI], 2.5–18.5 months) and 6.0 months (95% CI, 3.2–19.7 months), respectively. The 6-month PFS rates were 25% (95% CI, 0–55.0%). The median OS after initial diagnosis was 23.3 months (95% CI, 16.2–55.8 months). The grade 2 or 3 hematologic adverse events were identified in 7 of 8 patients, most of which might be due to ICE chemotherapy. The results of our retrospective analysis suggest that combination treatment with bevacizumab and ICE may be safe and beneficial in patients with recurrent glioblastoma.

Key words: recurrent glioblastoma, bevacizumab, ifosfamide, carboplatin, etoposide (ICE), second recurrence

Introduction

Glioblastomas are primary malignant brain tumors causing poor morbidity and mortality.[17] Current standard treatment in newly diagnosed glioblastoma includes radiotherapy with concomitant and adjuvant temozolomide following surgery. The median survival for patients with glioblastoma remains 14.6 months.[17] The biological nature of glioblastoma is extremely refractory and relapsing. However, there is no consensus on the optimal practice for patients with recurrent glioblastoma. In the literatures, there are many retrospective studies and prospective trials to treat recurrent glioblastoma. An alternative dosing schedule of temozolomide is a reasonable option in patients with glioblastoma who experience progression after conventional 150 or 200 mg/m^2 5/28 dosing schedule.[9,10,24] The RESCUE study showed clinical benefit with 6-month progression free survival (PFS) rates (PFS-6) of 17% and 23.9% with continuous dose-intense temozolomide 50 mg/m^2/d in recurrent glioblastoma.[9] The study of the "week on/week off" dosing schedule of temozolomide at a dose of 150 mg/m^2/day demonstrated clinical benefit with

Received June 11, 2013; Accepted July 17, 2013

a PFS-6 of 43.8% in recurrent glioblastoma.[24]

Based on the highly angiogenic nature of glioblastoma, anti-angiogenic targeted agents have been applied to a treatment approach. Bevacizumab is a humanized monoclonal antibody against the vascular endothelial growth factor.[22] First phase II study of bevacizumab and irinotecan in patients with recurrent malignant glioma showed clinical benefit with a PFS-6 of 38%.[16,19] Following studies showed the efficacy with a PFS-6 of 29–42.6% of single-agent bevacizumab in patients with recurrent glioblastoma who were treated with conventional management with temozolomide.[4,6] Japanese phase II study of single-agent bevacizumab in patients with recurrent malignant glioma also demonstrated a PFS-6 of 33.9%.[8] However, bevacizumab responses are rarely durable.[8,19,20]

Phase II study of ifosfamide, carboplatin, and etoposide (ICE) for recurrent glioblastoma showed a PFS-6 of 35% and mild adverse events.[1] In our institute, ICE is used as second-line chemotherapy in patients with first relapsing glioblastoma treated with conventional management with temozolomide. Bevacizumab has generally been used in combination with cytotoxic agents in the management of solid malignancies. Retrospective studies have shown that regimens containing bevacizumab and carboplatin were effective on recurrent glioblastoma.[3,7,11,12] Therefore, for patients with re-recurrent glioblastoma treated with ICE, we use another chemotherapeutic agents containing bevacizumab combination with ICE. Retrospectively, we investigated the feasibility and effectiveness of bevacizumab combined with ICE in patients with second recurrence of glioblastoma during ICE treatment following temozolomide failure.

Materials and Methods

Patient's demographics, clinical data, radiological, and histopathological findings, type of chemotherapy, number of chemotherapy cycles, and survival data were obtained retrospectively from our hospital medical records. We reviewed consecutive 8 patients diagnosed as second relapse of glioblastoma resistant to ICE, who were treated with bevacizumab in combination with ICE between 2010 and 2012. All patients had undergone previous surgery and were diagnosed histologically with glioblastoma. This retrospective analysis is in compliance with the Declaration of Helsinki (Sixth Revision, 2008). All data were collected retrospectively and in accordance with institutional ethical policies.

Patients were evaluated with magnetic resonance imaging (MRI) every 1 to 2 months or according to clinical symptoms after the initial treatment. Tumor recurrence was diagnosed by MRI and positron emission tomography imaging with 18F-fluorodeoxyglucose (18F-FDG). In the case with suspicious pseudo-progression, the adjuvant chemotherapy was continued.

The initial treatment following the first surgery were three types: radiotherapy with concomitant and adjuvant temozolomide,[17] radiotherapy concomitant and adjuvant nimustine, carboplatin, vincristine, and interferon-beta (VACferon) followed by adjuvant temozolomide, radiotherapy with concomitant and adjuvant temozolomide and interferon-beta.[21] All patients were diagnosed with first recurrence of glioblastoma and received ICE chemotherapy following surgical resection or/and stereotactic radiosurgery (35 Gy, 5 fractions) or no treatment. ICE regimen consisted of ifosfamide (750 mg/m^2/day on day 1, 2, and 3), carboplatin (75 mg/m^2/day on day 1, 2, and 3), and etoposide (75 mg/m^2/day on day 1, 2, and 3) in every 4–6 weeks.[1] All patients were diagnosed with second recurrence of glioblastoma refractory to ICE and received 3 cycles of 10 mg/kg bevacizumab, every two weeks, in combination with the same regimen of ICE as before.

The objective response rate (ORR) to treatment was assessed using the Response Assessment in Neuro-Oncology Working Group (RANO criteria).[23] We evaluated contrast-enhanced T_1-weighted images and fluid attenuated inversion recovery (FLAIR) images at the second relapse and after 3 cycles of bevacizumab. Both complete and partial responses were considered objective responses. Toxicity was evaluated after 3 cycles of bevacizumab according to the National Cancer Institute Common Toxicity Criteria (CTCAE) version 4.0. PFS was measured from the date of image diagnosis to the date of disease progression or death. Patients alive and progression free at last contact are treated as censored in the PFS analysis. Overall survival (OS) was defined as the time from the date of diagnosis to the date of death or last contact. The Kaplan–Meier method was used to estimate survival, which was measured from the time of diagnosis to the date of death. Statistical analyses were with PRISM version 5.0 (GraphPad Software Inc., La Jolla, California, USA).

Results

The characteristic features of 8 patients analyzed in this study are summarized in Table 1. There were 6 males and 2 females, and the median age was 53 years. Six patients received radiotherapy (60 Gy, 30 fractions) with concomitant and adjuvant temozolomide as the initial treatment. Exceptionally,

Table 1 Demographic characteristics of patients With second recurrence of glioblastoma

Case	Age	Sex	First chemotherapy	Radiation (Gy)	First chemotherapy (cycle number)	Salvage treatments at first relapse	ICE cycle number at second relaspe	Salvage treatments at second relapse	KPS at second relapse (%)
1	60	M	VACferon	59.4	VACferon (6), TMZ (27)		6		60
2	27	F	TMZ	60	TMZ (12)	Surgery	12	Surgery	80
3	52	M	TMZ	60	TMZ (11)	Surgery	8		50
4	47	M	TMZ	60	TMZ (6)	Surgery	3		70
5	67	F	TMZ	60	TMZ (7)	Surgery, SRT 35Gy	2		60
6	64	M	TMZ+IFN	60	TMZ+IFN (5)		2		50
7	62	M	TMZ	60	TMZ (16)	SRT 35Gy	4		70
8	51	M	TMZ	60	TMZ (4)	Surgery, SRT 35Gy	4		60

F: female, KPS: Karnofsky performance status, M: male, SRT: stereotactic radiosurgery, TMZ: temozolomide, VACferon: nimustine, carboplatin, vincristine, interferon-beta.

one patient, Case 1, was received ACNU regimen of VACferon with radiotherapy followed by adjuvant temozolomide. Another patient, Case 5, was received interferon-beta in combination with the conventional management with radiotherapy and temozolomide. After the first recurrences were recognized during temozolomide treatment, three patients (Cases 2–4) had tumor resection, two (Cases 5 and 8) had tumor resection followed by stereotactic surgery for the residual tumor (35 Gy, 5 fractions), and one patient (Case 7) had only stereotactic surgery (35 Gy, 5 fractions). All patients were treated with ICE chemotherapy after temozolomide failure. At second relapse diagnosed during ICE treatment, 3 cycles of 10 mg/kg bevacizumab in every two weeks were administered. The median values of Karnofsky Performance status were 60 (50–80). The cycle numbers of ICE were 2–12 before the second relapse of glioblastoma. Only one patient (Case 2) had tumor resection before administration of bevacizumab.

Clinical results in 3 cycles of bevacizumab combination in patients with second recurrence of glioblastoma resistant to ICE are summarized in Table 2. The ORR of bevacizumab including complete response and partial response was 75% in RANO criteria (Fig. 1, Case 2). The median PFS and OS after bevacizumab in combination with ICE were 3.7 months (95% confidence interval [CI], 2.5–18.5 months) and 6.0 months (95% CI, 3.2–19.7 months), respectively. The PFS-6 rates were 25% (95% CI, 0–55.0%). The median OS after onset was 23.3 months (95% CI, 16.2–55.8 months). Two patients (Cases 2 and 7) were treated with additional bevacizumab at third relapse of glioblastoma.

Bevacizumab in combination with ICE did not produce any acute toxic events. Hematologic and nonhematologic grade 2 or 3 adverse events are showed in Table 3. There was no grade 4 or higher adverse events except in one patient (Case 1). The death of the patient (Case 1) was not related to chemotherapy. Hematologic toxicities were identified in 7 of 8 patients and comprised 60% of the grade 2 or 3 adverse events. These adverse events were thought to be attributed to ICE chemotherapy. Cerebral hemorrhage, hypertension, proteinuria, and venous thromboembolism more than grade 3 were not identified in this series.

Discussion

This is the first report to evaluate combined administration with bevacizumab and ICE in patients with second recurrence of glioblastoma during ICE treatment, although it is retrospective analysis in small number cases. These results indicated that bevacizumab combined with ICE improved clinical deterioration in 6 of 8 patients with glioblastoma at second relapse. Furthermore, this combination therapy did not cause any severe adverse events, which means that bevacizumab is well tolerated although during ICE chemotherapy.

Bevacizumab is widely used in recurrent glioblastoma, alone or in combination with other agents. In the meta-analysis of bevacizumab effect for recurrent glioblastoma using 15 studies published

Table 2 Results of bevacizumab in combination with ICE in patients with second recurrence of glioblastoma

Case	Bevacizumab cycles	ICE cycle number after second relaspe	RANO criteria	OS from the initial diagnosis	OS from ICE (months)	OS from bevacizumab (months)	Current status
1	3	2	PR	55.2	8.4	1.6	Dead
2	3 + 4	10	PR	44.2	30.2	18.7	Dead
3	3	17	PR	55.8	45.2	33.0	Alive
4	3	6	PR	20.2	11.1	8.0	Dead
5	3	1	SD	16.6	7.6	3.0	Dead
6	3	2	PR	16.2	8.4	4.8	Dead
7	3 + 2	3	PR	26.3	9.3	6.3	Dead
8	3	3	SD	16.4	9.6	5.6	Dead

ICE: ifosfamide, carboplatin, and etoposide, OS: overall survival, PR: partial response, RANO criteria: Response Assessment in Neuro-Oncology Working Group, SD: stable disease.

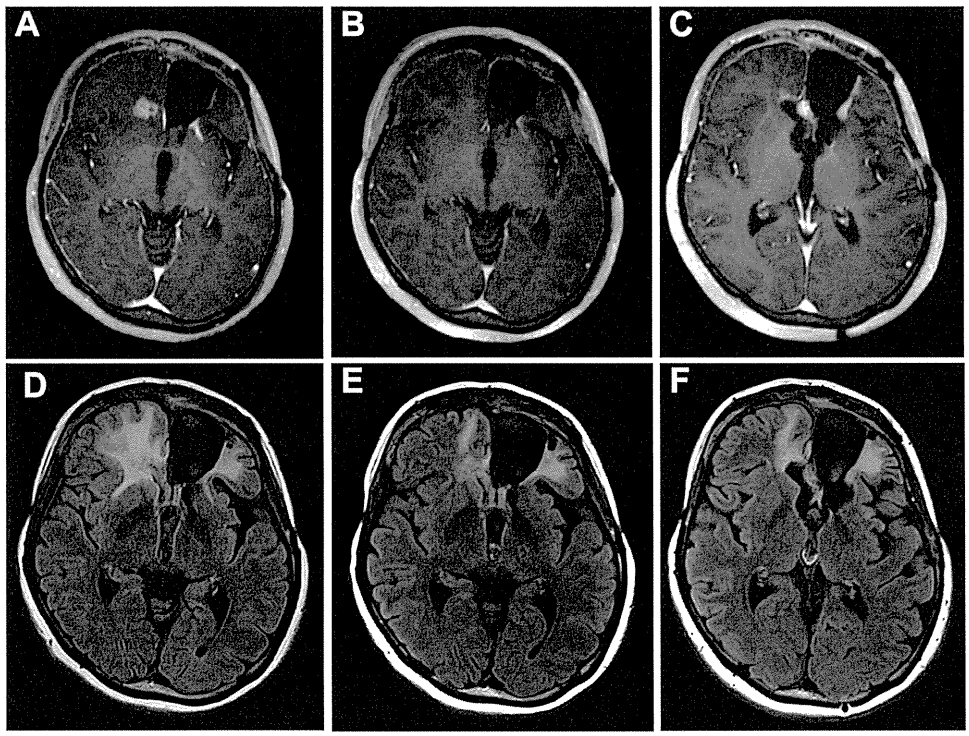

Fig. 1 Illustrative Case 2, 27-year-old female. A, D: Glioblastoma of the patient had rapidly regrown after the third surgery for her second relapsing tumor resistant to ICE. B, E: Her lesion was decreased after 3 cycles of 10 mg/kg bevacizumab combined with ICE. C, F: Her lesion recurred after 3 cycles of ICE following bevacizumab. A, B, C: contrast-enhanced T_1-weighted images. D, E, F: fluid attenuated inversion recovery images. ICE: ifosfamide, carboplatin, etoposide.

from 2005 to 2009, PFS-6 was 45%. The median OS was 9.3 months. The response rate analysis demonstrated 6% complete response, 49% partial response, and 29% stable disease.[25] Japanese phase II study of single-agent bevacizumab showed that PFS-6 was 33.9% and median OS was 3.3 months in 29 patients with recurrent glioblastoma.[8] In our analysis of bevacizumab in combination with ICE chemotherapy, PFS-6 was 25% and median OS was 6.0 months. Regarding the survival endpoints, our results seem to be worse than previously published data. It was a primary factor that the